Proceedings of the 11th Brazilian Congress of Thermal Sciences and Engineering – ENCIT 2006
Braz. Soc. of Mechanical Sciences and Engineering – ABCM, Curitiba, Brazil, Dec. 5-8, 2006

Paper CIT06-0269

COMPUTATIONAL SIMULATIONS OF HIGH-LIFT CONFIGURATIONS USING UNSTRUCTURED GRIDS

João Alves de Oliveira Neto
Instituto Tecnológico de Aeronáutica, CTA/ITA/IEE, 12228-903 - São José dos Campos - SP - Brazil
alves@ita.br

Darci Cavali
Universidade do Vale do Paraíba, UNIVAP, São José dos Campos - SP - Brazil
darcicavali@gmail.com

Carlos Breviglieri Júnior
Universidade do Vale do Paraíba, UNIVAP, São José dos Campos - SP - Brazil
carbrevi@gmail.com

João Luiz F. Azevedo
Instituto de Aeronáutica e Espaço, CTA/IAE/ASA-L, 12228-900 - São José dos Campos - SP - Brazil
azevedo@iae.cta.br

Ana Lúcia Fernandes de Lima e Silva
Universidade Federal de Itajubá, UNIFEI, Itajubá - MG - Brazil
alfsilva@unifei.edu.br

Abstract. *The purpose of the present work is to perform a study of high-lift devices using CFD simulations in order to attempt to establish guidelines for the analysis of such systems through computational aerodynamic techniques. Flowfields over high-lift systems are characterized by highly complex flow physics, which pose significant challenges for CFD codes. For this purpose, results for several high-lift devices will be obtained using a CFD code currently under development by the group and these results will be compared with data available in the literature and/or with computational results obtained using well-established commercial codes. The study will look into 2-D and 3-D configurations, under high-lift conditions, and assess the capability of predicting lift, drag and pressure coefficients for such configurations. As usual with RANS simulations for such high Reynolds number flows, the addition of turbulence models is required in order to capture the correct turbulent transport. In the present case, the use of both the Spalart-Allmaras (SA) one-equation and the Menter SST (SST) two-equation models is envisioned. These calculations will be compared to the available data in order to assess the accuracy of the capability implemented as well as to validate the computational tool under development.*

keywords: *high-lift configurations, aerodynamic coefficients, CFD, maximum lift.*

1. Introduction

The design of an optimized high-lift system is an important part of the development of a modern transport aircraft. The manufacturers must make simple yet efficient high-lift designs, and in particular they must avoid having to make large and expensive changes in a late project stage. The cost and Reynolds number scaling problems involved in the optimization of slat and flap positions by wind tunnel tests is a strong driver in the effort to develop CFD tools which can be used in the design process. This paper describes one step on the road to establish CFD analysis tools for high-lift aerodynamics, by development methods and validation of two-dimensional high-lift CFD analysis.

High-lift flows are inherently three-dimensional and a complete study should include the modeling and analysis of such effects. However, several aspects of high-lift flows may be understood by simplified two-dimensional analysis. Figure (1) points to a number of important flow phenomena which govern the behavior of the flow over a two-dimensional high-lift configuration. Viscous interaction effects are responsible for the most important limiting aspects of the flow. The confluence of the wake of one element with the suction side boundary layer of the following elements plays an important role in determining maximum lift. Massive flow separation on one or more of the elements may, depending on operational condition, set the maximum lift which can be obtained. The fact that many parts of the flow develop in strong adverse pressure gradients increases the modeling difficulties. The knowledge of turbulence development in adverse pressure gradients is much less developed than it is for zero pressure gradient flows. Most turbulence models used in Reynolds

averaged computational methods are calibrated in zero pressure gradient flows, with more or less *ad hoc* modifications to account for the development of turbulence in adverse pressure gradient regions. Many effects in high-lift flows are

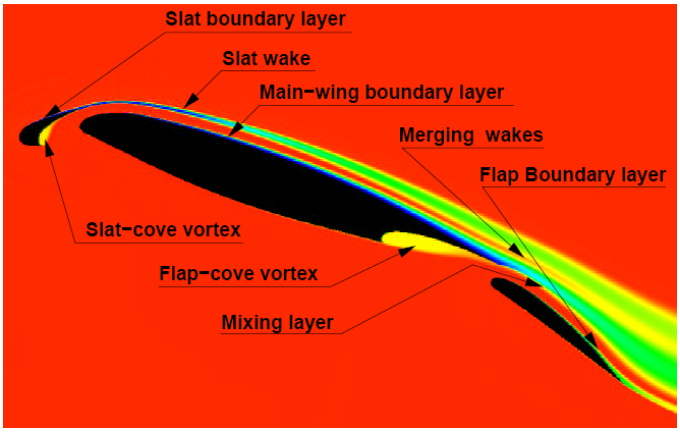

Figure 1: Important flow phenomena in two-dimensional high-lift aerodynamics.

governed by the detailed transition process. This can be quite different in wind tunnel tests taken at lower Reynolds number compared to the flight situation. Several mechanisms may cause the transition from laminar to turbulent flow. Transition may occur by a laminar separation bubble which reattaches as a turbulent boundary layer. Even though the typical take-off or approach speeds are quite low, there may be transonic effects on a slat, so that the flow may be strongly affected by shock-wave boundary layer interaction. With the known limitations of two-dimensional analysis in mind, the results are still quite useful in project design phases and to increase the understanding of the governing flow phenomena.

The computational tools available range from the more efficient and simpler inviscid/viscous coupled methods, to a Reynolds-averaged Navier-Stokes (RANS) analysis. An example of the former method is given by the MSES code (Drela, 1996). It is based on the solution of the Euler equations coupled with the boundary layer equations. These methods have been found to be successful in accurately computing the pressure distribution for multi-element airfoils, including cases up to maximum lift, some of which involve separation. The coupled method has been proven to be useful as an effective engineering design tool. Unfortunately, this method is limited by its inability to compute beyond maximum lift conditions, and it may have problems with certain features of some airfoil systems such as flap wells, thick trailing edges, or unsteady effects. The performance of high-lift configurations, especially close to stall, can be difficult to predict and requires the solution of, at least, the Reynolds-averaged Navier-Stokes equations with an appropriate turbulence model. This is an expensive computational task which is made even more time consuming by the need of generating a field grid. High-lift configurations are usually complex geometries, at which complex flow physics are present. The work here described uses the MSES and CFD++ (CFD++, 2005) codes, as well as an in-house developed code, to simulate flows around high-lift aerodynamic configurations aiming at the prediction of lift and pressure coefficient distributions. In order to understand the flow physics over high-lift devices, three configurations are chosen for the studies to be performed in the present context. The multi-element airfoils selected were the NLR 7301 (den Berg and Gooden, 1994) and NHLP-2D (Moir, 1994) airfoils. Moreover, a 3-D configuration based on the RAE 1372 (Lovell, 1977) profile was also selected. Such configurations were chosen based on availability of geometry and experimental data for the flight conditions of interest for the present simulations.

2. High-Lift Configurations: Geometry, Grid Generation and Boundary Conditions

Geometry of the 2D profiles was obtained in coordinate files and the trailing edges were not collapsed in either airfoil. Mesh generation was performed with ANSYS ICEM CFD (ICEM, 2005). The work has analyzed several geometric parameter variations in order to verify their influences on the final CFD result. For instance, such studies considered the effects of farfield distance, boundary layer grid resolution and general mesh refinement, as well as the overall mesh topology.

Three geometries and flow conditions are considered in the present effort. These include subsonic flows over an NLR 7301 airfoil, an NHLP-2D airfoil and an RAE 1372 configuration. The following specific test cases are considered:

- Simulations of subsonic flows about the NLR 7301 airfoil. The simulations for this case are performed for Reynolds number Re = 2.51 x 10^6 and freestream Mach number $M_\infty = 0.185$. Numerical results are compared to available experimental results in order to assess the correctness of the present simulations. A representative mesh over the NLR 7301 profile is shown in Fig. (2). In the particular case of this figure, a triangular grid is shown. However, both triangular and quadrilateral meshes were generated for this configuration.

- Simulations of subsonic flows about the NHLP-2D airfoil. The simulations for this case are performed for Reynolds number Re = 3.52 x 10^6 and freestream Mach number $M_\infty = 0.197$. Numerical results are also compared to available experimental results. A representative grid over the NHLP-2D profile is also shown in Fig. (2). In this case, a quadrilateral mesh is shown in Fig. (2), but as before both triangular and quadrilateral meshes were generated for this configuration.

- Simulations of subsonic flows about an RAE 1372 configuration (Lovell, 1977). The simulations for this case are performed for Reynolds number Re = 1.35 x 10^6 and freestream Mach number $M_\infty = 0.223$. The geometry of the wing profile was obtained from (Lovell, 1977), along with the parameters to construct the 3-D wing in a CAD environment. The wing features a slat and double flap configuration, with 31 deg. of leading edge sweepback and high-lift devices along the complete semi-span. However, it should be emphasized that the present study only analyzed this wing in the cruise configuration. Such approach was chosen in order to address the 3-D high-lift configuration in an incremental manner, and the results here reported represent the current status of such development in the group. In this context, the discussion of the present 3-D results should be seen as a work-in-progress report of such development. Nevertheless, a tetrahedral mesh with a total of 3,375,912 control volumes was generated for this configuration, including both the wing, in cruise condition, and the fuselage. Such a fairly fine grid was required in order to appropriately discretize the wing trailing edge. A view of the mesh over the RAE 1372 configuration is also shown in Fig. (2). It should further emphasized that, although the current simulations for this configuration are considering a tetrahedral grid, it is possible that further studies in the future will also include hexahedral meshes for this configuration, in order to improve mesh quality and robustness. The surface and volumetric meshes for the configuration were also generated using the ICEM CFD software.

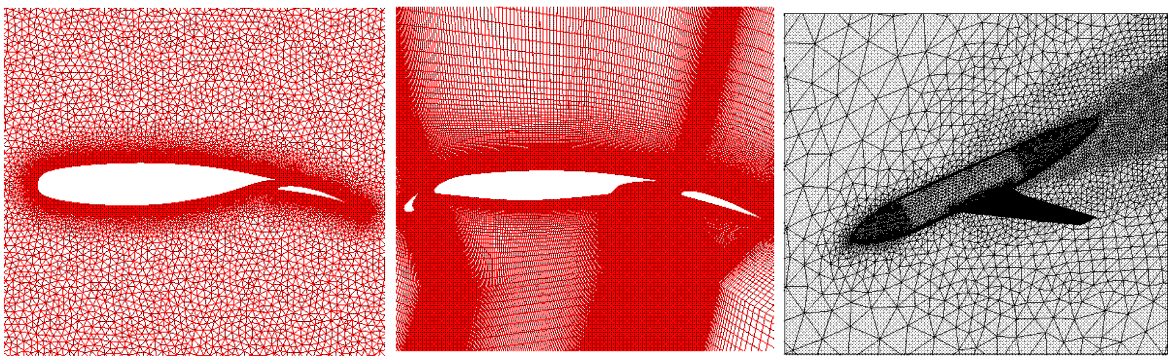

Figure 2: Grids on the studied configurations.

Due to the space limitations in the present paper, the authors will not be able to include all the results concerning grid refinement and grid topology influence. Hence, a brief summary of such results is included in the remainder of this section, in order to allow the discussion of the aerodynamic results in the forthcoming sections. For instance, the current simulations have indicated that the farfield boundary should be placed, at least, at approximately 100 chord lengths from the configuration in order to avoid any influence of farfield position on the aerodynamic results. Moreover, it was also found, as one should expect, that boundary layer resolution has a crucial effect in the final result. Therefore, adequate grid refinement inside the boundary layer, as well as an appropriate, *i.e.*, sufficiently mild, grid stretching as one moves away from the wall are necessary for resolving the flow over high-lift airfoils. The results obtained so far seem to indicate that quadrilateral meshes, in 2-D, and hexahedral meshes, in 3-D, are better suited for high-lift CFD analyses, since such grid topologies lend themselves, in an easier fashion, for ensuring mesh orthogonally or, at least, a lower level of grid skewness. Hence, in this context, such topologies clearly contribute to overall grid quality.

Moreover, another aspect that deserves attention concerns a consistent method for studying convergence of the computed solutions with increasing grid density. Consistency of the grid system is difficult to achieve in analyzing high-lift flows. The difficulty arises out of the need to ensure sufficient grid density in regions of interesting flow phenomena while preventing deterioration of grid density and smoothness in other areas of the flow. The problem is further compounded by a lack of guidelines regarding grid resolution requirements for the complex flow physics involving disparate length scales that arise in flowfields of multi-element, high-lift configurations. In particular, the grid requirements for adequate capture of the wakes of upstream elements and/or the merging of wakes of different elements are quite stringent.

3. Flow Solution Method

3.1. Simulation Conditions

Usually, the solving step in the simulation process consumes most of the time. In order to know the number of simulations and flow conditions in this phase to dimension the time to dispend, it is indicated to have an estimation of expected results. In the early stages of the preliminary design of an airplane, some of the aerodynamic coefficients are already know due to a certain airplane performance that has to be achieved. In particular, the high-lift devices are intrinsically connected with the landing and the take-off performance. This two phases of the airplane mission are very important due to the operational implications that they have. An overestimated take-off lift coefficient maximum implicates in limitations in the maximum weight to take-off, or the need for an longer track. In the same way, an overestimated landing lift coefficient maximum implicates in the necessity for a longer track. The aerodynamic coefficients are directly influenced by the flow conditions (speed, altitude, temperature, etc), angle of attack and elements individual displacement parameters (gaps and overlaps). The designer must opt for the configuration where maximum lift coefficient is achieved, and to do so the number of simulations, combining all the cited parameters and conditions can grow out of limit on design time and costs to compute all the possible combinations. A solution must be addressed to reduce simulation time mainly. The codes to simulate flows around aeronautic configurations aiming prediction of drag, lift and pressure coefficients to evaluate how codes is inserted in the main objective of this collaboration, and which consists in getting the aerodynamic coefficients as real as possible.

3.2. MSES Code

The MSES code is a two dimensional analysis, design and optimization framework for multi-element airfoil sections. It is based on the steady state conservative Euler equations. The Euler equations are used to describe the inviscid part of the flow. The assumption that the viscous part is restricted to a thin boundary layer and wake is made, and the viscous part is described with the boundary layer theory given by the integrated Prandtl boundary layer equations (White, 1991). The equations are discretized in an intrinsic grid, where one set of coordinate lines correspond to the streamlines around the body. With this procedure the number of unknowns per grid node is reduced from four to two because the continuity equation and the energy equation can be replaced by the simple condition of constant mass flux and constant stagnation enthalpy along each streamtube. The Newton method is used for solving the system of nonlinear equations. Simulations are performed quickly and the aerodynamic coefficients are obtained. A comparison of experimental data and the MSES code results are presented in the present paper.

3.3. CFD++ Code

The CFD++ code (CFD++, 2005) allows easy treatment meshes of complex geometries mainly due to its integration of structured, unstructured and multi-blocks grids. Its flexibility allows the use of various elements within the same mesh such as hexahedral, triangular prism and tetrahedral elements in 3-D. However, as usual with RANS simulations for such high Reynolds number flows, the addition of turbulence models is required in order to capture the correct turbulent transport. In the present report, the use of both the Spalart-Allmaras (SA) one-equation and Menter SST (SST) two-equation models is foreseen.

4. Results and Discussion

NLR 7301 Airfoil

The NLR 7301 is supercritical airfoil/flap configuration with 32% chord flap and considering a $\delta_f = 20^o$ flap deflection. In this present study, two different configurations are evaluated. The first analysis is performed for the configuration with a flap gap of 1.3% and the second one with the flap gap of 2.6%. In the present simulation, a triangular and quadrilaterals grid was used with 200,229 elements. The gap is defined as the radius of the circumference centered in the trailing edge of the main element and tangent to the flap profile in a certain point. This point of tangency is defined by the overhang, which is held at a constant at a value of 5.3% for both test cases here considered. It worth to mention that the gap and the overhang are defined as a percentage of the nominal profile cruise chord. The flap lower surface exhibited laminar flow at all times. The main element and flap boundary layers were found to be confluent for the flap gap of 1.3%. Simulations of subsonic flow over NLR 7301 profile were computed with freestream Mach number $M_\infty = 0.185$ and Re = 2.51 x 10^6, using inviscid and viscous flow. In these simulations both Spalart-Allmaras (SA) and Menter SST (SST) turbulence models are exercised, as a form of comparing their results. In Fig. (3), one can observe the pressure contours over NLR 7301 airfoil obtained in the present calculations for the SA turbulence model. The lift coefficient as a function of angle of attack can be observed in detail in Fig. (4). This figure compares SA and SST turbulence models and the MSES code with the experimental data. Comparison of experimental and calculated lift coefficients also show good agreement

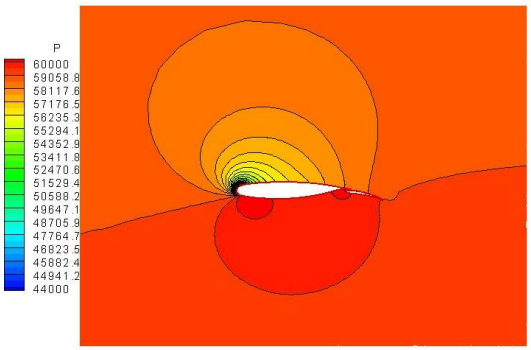

Figure 3: Pressure contours using SA turbulence model for α = 13.1^o and Re = 2.51 x 10^6 for the NLR 7301 airfoil.

which is a clear indication of the good quality of the results that can be obtained with the CFD++ numerical tool. One can observe in this figure that the numerical distributions compare very well with experimental data, less the MSES code. The relative worse agreement of predicted and experimental lift coefficient values for the configuration with 1.3% gap may be attributed to a greater sensitivity of this case to the boundary layer development. In the actual experiment, the literature (den Berg and Gooden, 1994) indicates that there is laminar flow on the flap upper surface and, also, that the boundary layer relaminarizes in the flap cove region. However, none of these effects is correctly simulated with the current RANS solutions since both turbulence models used, i.e., SA and SST models, assume fully turbulent flow. The lift coefficient

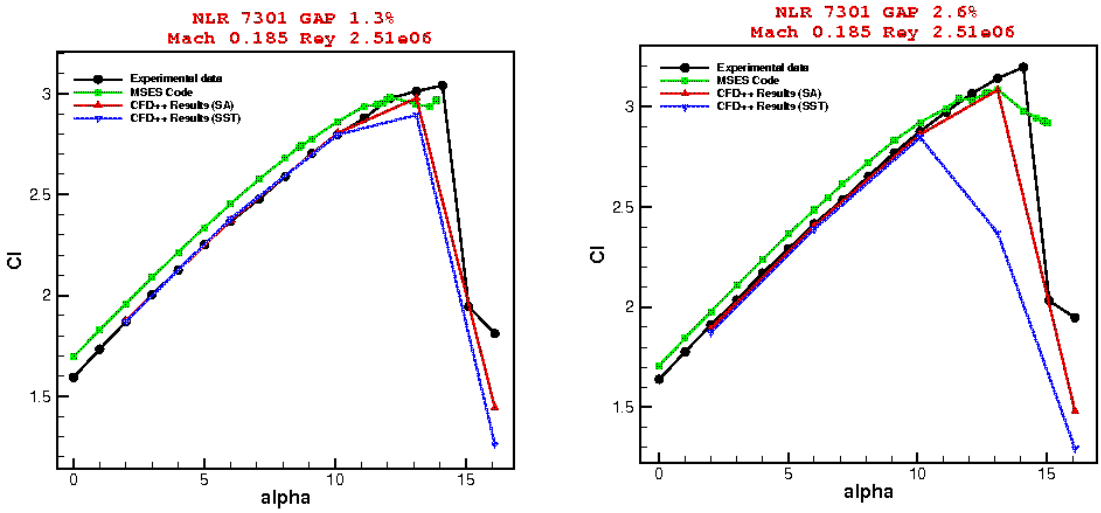

Figure 4: The lift coefficient as a function of the angle of attack with Mach number 0.185 for NLR 7301 gap 1.3% and 2.6%.

as a function of angle of attack can be observed in detail in Fig. (4) for NLR 7301 (2.6% gap). This figure compares SA and SST turbulence models and the MSES code with the experimental data. In Fig. (4), as in the NLR 7301 airfoil (1.3% and 2.6% gap) study the MSES results also present an overprediction of lift coefficient for this geometry. Due to the complexity of this simulated geometry, the differences in the lift coefficient as a function of angle of attack curve seem to have been more accentuated. For an perfect match with the experimental results, all the complex physics has to be perfectly capture. This includes the flow features at the cove of the main element, as well as the interactions between the free shear layer of the main element and the boundary layer of the flap.

MSES code show a good capability to effectively reproduce the experimental data at the linear range. The limitations presented in the non-linear region are intrinsic to the MSES formulation (Lima-Silva *et al.*, 2005), as well the lack of a better control in relation to the mesh generation. This verification does not take the merits of the code since even other numerical codes with a formulation more adequate, Navier-Stokes an turbulence model, presents the same difficulty to present the aerodynamic coefficients with accuracy. The experimental results are available (den Berg and Gooden, 1994).

The numerical pressure coefficient distribution shows an excellent agreement with the experimental data for the evaluated angles of attack. Figure (5) for flap gap 1.3% at an angle of attack of $\alpha = 6^o$, the comparison between the numerical and the experimental pressure coefficient distribution.

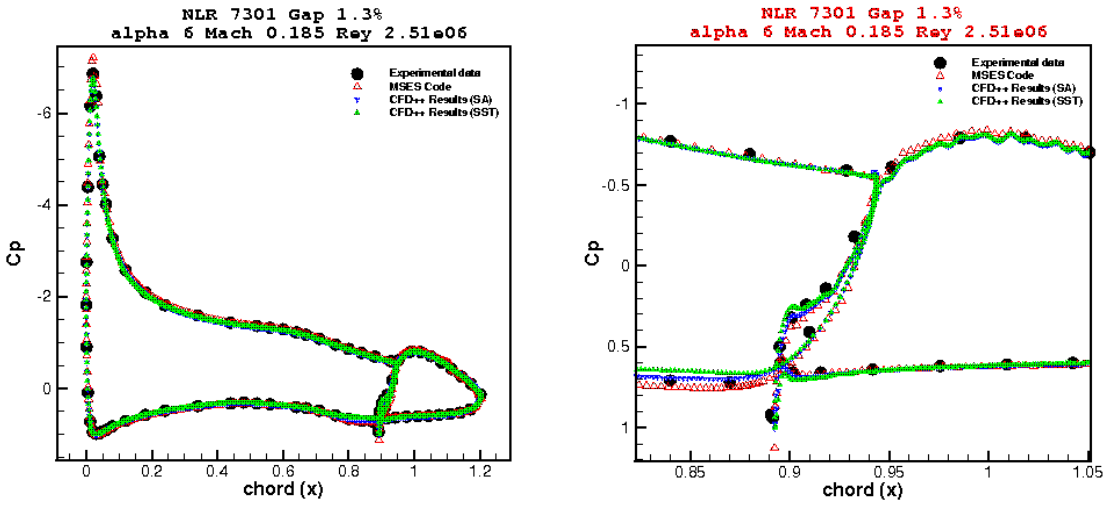

Figure 5: The pressure coefficient as a function of the chord with $\alpha = 6^o$ for NLR 7301 gap 1.3%.

In Fig. (5), one can observe the difference in the C_p distributions in the region of the cove. In Fig. (6), one can observe the comparison for an angle of attack of $\alpha = 13.1^o$. In Fig.(6), one can observe the difference in the C_p distributions in the region of the cove for $\alpha = 13.1^o$

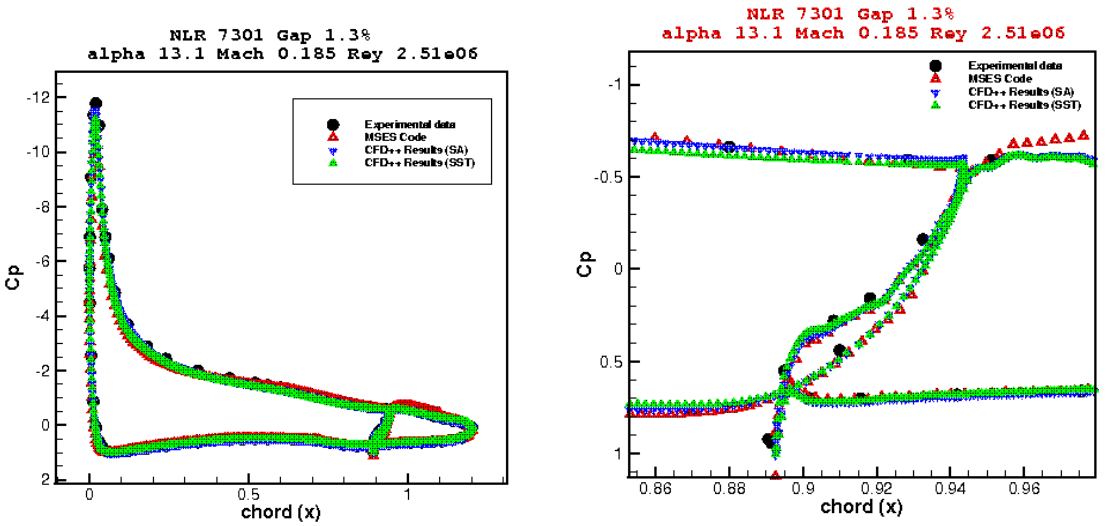

Figure 6: The pressure coefficient as a function of the chord with $\alpha = 13.1^o$ for NLR 7301 gap 1.3%.

NHLP-2D Airfoil

The NHLP-2D airfoil is again a supercritical airfoil with a high-lift devices, including a 12.5% leading-edge slat and a 33% single-slotted flap (Moir, 1994). For the results showed here, the slat and flap are deflected 25 and 20 deg., respectively, which is typical of take-off configurations with leading-edge stall. In the present simulation, a triangular and quadrilaterals mesh was used with 148,014 elements. Simulations of subsonic flow over NHLP-2D profile were computed with freestream Mach number $M_\infty = 0.197$ and Re = 3.52 x 10^6, using inviscid and viscous flow. Comparison of experimental and calculated lift coefficients also show good agreement, which is a clear indication of the good quality of the results that can be obtained with the CFD++ numerical tool. The NHLP-2D airfoil illustrated in Fig. (7) shows

the flow over a typical high-lift airfoil with a leading edge slat and a single-slotted flap. The total pressure profiles as a

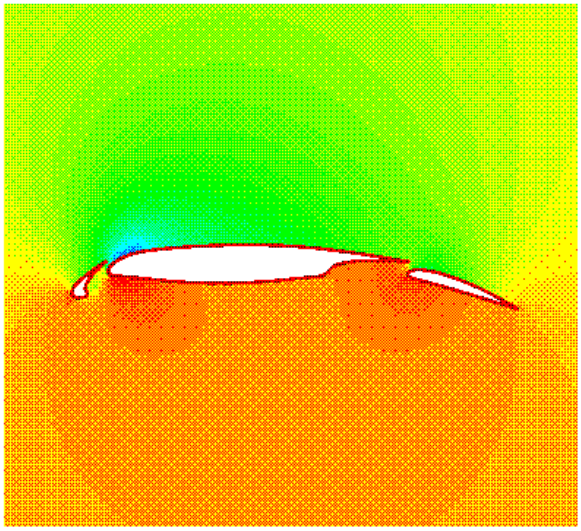

Figure 7: Pressure contours using SA turbulence model for α = 4^o and Re = 3.52 x 10^6 for the NHLP-2D airfoil.

function of chord is shown in Fig. (8). The numerical results obtained by Morrison (Morrison, 1998) using the Wilcox k - ω turbulence model are also presented together with experimental data (Moir, 1994). The plot at x/c = 0.35 shows the

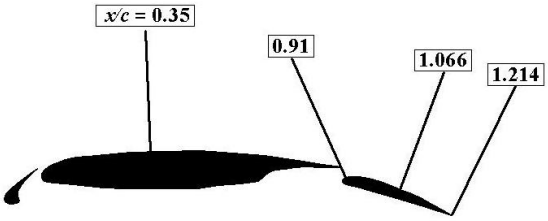

Figure 8: Location of total pressure profiles for NHLP-2D airfoil.

slat wake and the boundary layer on the main element in the Fig. (9). The experimental data is more sparse in the region of the slat wake and shows a narrow and weak wake compared with the numerical results. The results of Morrison predict a the slat wake too large. The plot at x/c = 0.91 and other downstream positions show the merging of the slat and main element wakes as described in Fig. (9). A distinct slat wake is predicted in the outer edge of the main element boundary layer all the way to the flap trailing edge in Fig. (10).

The pressure coefficient results are shown for the three elements for $\alpha = 4^o$ in Fig. (11). The numerical results better compared with the experimental results at the main element and at the flap. It will be seen that the trailing-edge of the slats sits in the high-velocity region of the flow around the leading edge of the main wing. Because of this, the pressure coefficient at the trailing edge is significantly negative and thus the pressure rise on the slat is reduced. The same happens at the trailing-edge of the main wing due to the high velocities around the leading-edge of the highly deflected flap.

In addition, the circulation around the slat induces a downwash on the main wing. This downwash clearly reduces with distance from the slat, so that it modifies the local velocities most strongly near the leading-edge of the wing, reducing it is peak suction markedly. The same mechanism operates near the leading-edge of the flap. As a result of this, the pressure rise to the trailing-edge of the overall wing split up into a number of smaller pressure rises, when each of these is sufficient to just cause separation of the boundary layer, the overall pressure rise can clearly be very large.

RAE 1372 Configuration

Simulations of subsonic flows about a RAE 1372 configuration (Lovell, 1977). The simulation for this case is performed for Reynolds number Re = 1.35 x 10^6 and freestream Mach number $M_\infty = 0.233$. Numerical results are considered in order to evaluate the correctness of the validation. A detail extremely important that verified it is that the results with wing-fuselage are merely qualitative. In fact, the configuration of the fuselage it is not given in details in the

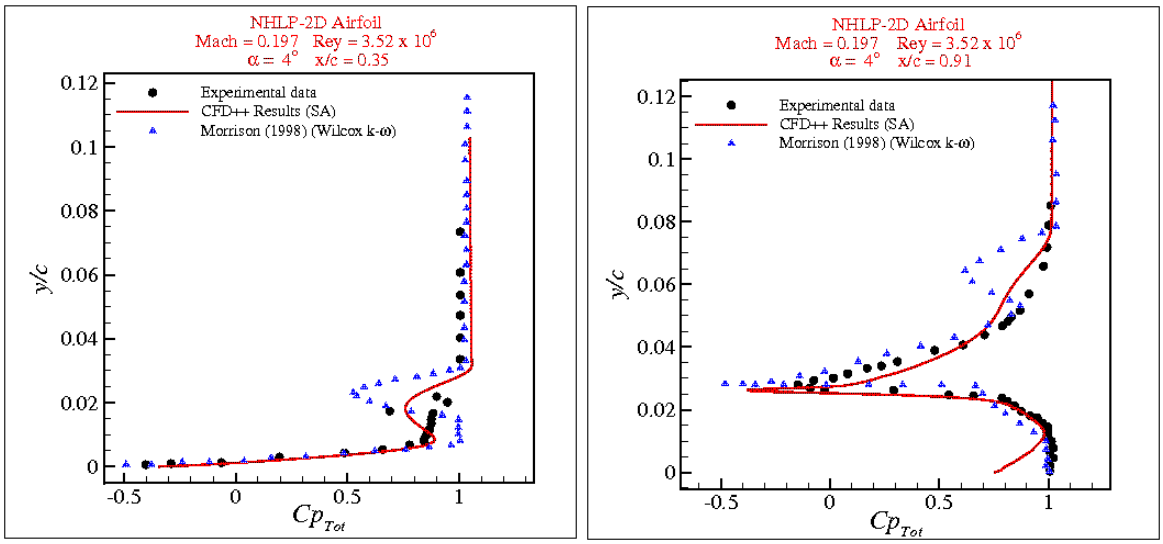

Figure 9: Total pressure profile at x/c = 0.35 (left) and x/c = 0.91 (right).

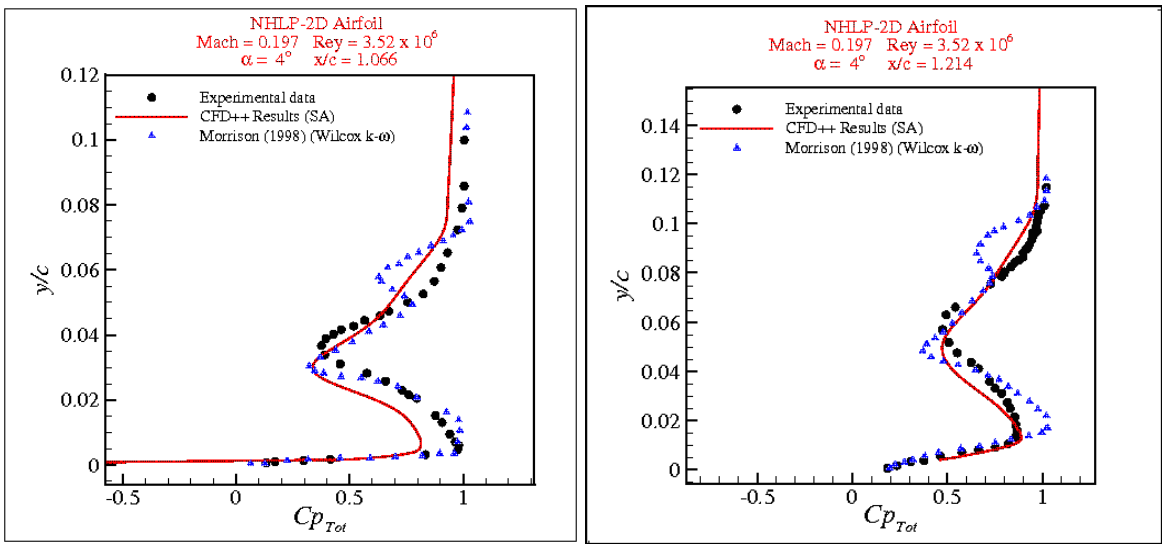

Figure 10: Total pressure profile at x/c = 1.066 (left) and x/c 1.214 (right).

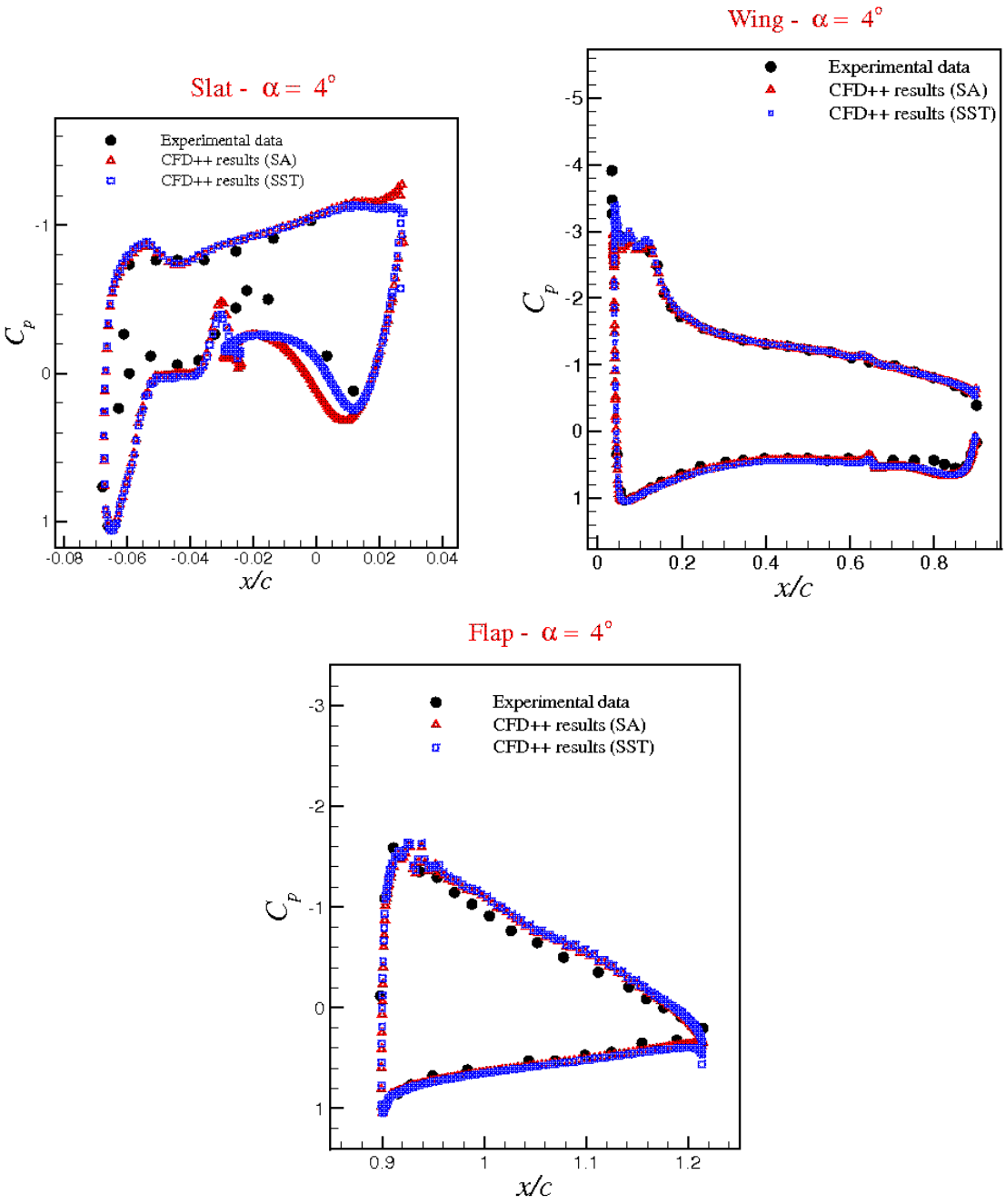

Figure 11: Pressure coefficient at the three elements for $\alpha = 4^o$ and Re = 3.52 x 10^6 for the NHLP-2D airfoil.

reference base, but the group did an approach judging to be interesting to analyze that case. Later, we will have quantitative results, because they will be just made simulations with the wing, disrespecting the fuselage. The Fig. (12) it shows pressure and mach contours for $\alpha = 0.05^o$, $M_\infty = 0.223$ and Re = 1.35 x 10^6 such for the Spalart-Allmaras turbulence model. Comparison of experimental and calculated lift, drag and moment coefficients also show good agreement which is a clear indication of the good quality of the result that can be obtained with the CFD++ numerical tool.

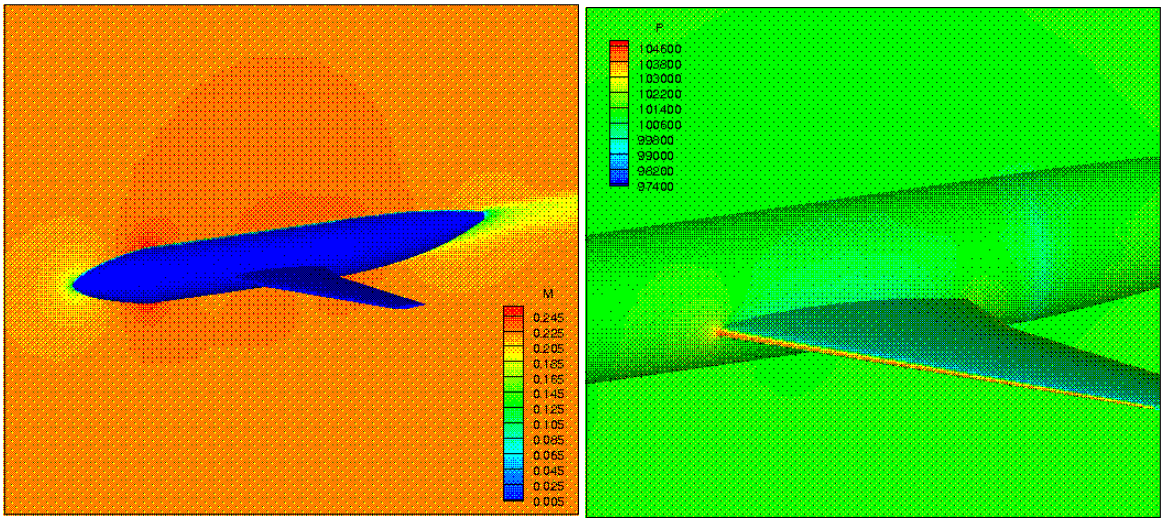

Figure 12: Mach contours using SA turbulence model for α = 0.05^o and Re = 1.35 x 10^6 for the RAE 1372 configuration.

Table 1: Aerodynamic coefficients.

Aerodynamic Coefficients	C_L	C_D	C_M
Experimental Data	0.118	0.0092	-0.0528
Numerical Data	0.1123	0.007324	-0.05716

In Tab. (1), the results for the aerodynamic coefficients at $\alpha = 0.05$ deg. are presented. Although the results are rather preliminary, one can observe a fairly good agreement with the experimental data (Lovell, 1977). One should observe, however, that only qualitative comparisons are actually reasonable at this point due to the following reasons:

- The 3-D configuration, including fuselage and wing, is only an approximation of the real configuration and, therefore, the final result is affected;
- A large portion of the area of the fuselage is a cylinder, because the original reference (Lovell, 1977) does not give the exact configuration. Hence, the authors have used the reported fuselage diameter in order to define a cylindrical fuselage. It is hoped that the use of the correct fuselage diameter at the wing-fuselage junction will minimize the errors so incurred.

5. General Remarks

In the present paper, simulation results obtained with the SA and SST turbulence models are presented. Three geometries are considered in the present effort. These include a NLR 7301 airfoil, a NHLP-2D airfoil and an RAE 1372 airfoil-based wing configuration. The following test cases are considered:

- Simulations of subsonic flows about the NLR 7301 airfoil. The simulations for this case are performed for Reynolds number Re = 2.51 x 10^6 and freestream Mach number $M_\infty = 0.185$. Numerical results are compared to available experimental data in order to assess the agreement obtained in this case.
- Simulations of subsonic flows about the NHLP-2D airfoil. The simulations for this case are performed for Reynolds number Re = 3.52 x 10^6 and freestream Mach number $M_\infty = 0.197$. Numerical results are again compared to available experimental data.

- Simulations of subsonic flows about an RAE 1372 configuration, considering Re = 1.35 x 10^6 and $M_\infty = 0.223$.

The paper provides a detailed comparison of the Spalart-Allmaras and Menter SST turbulence models in the context of two-dimensional high-lift aerodynamic flows. The results show that the Menter model is more accurate in separated flow regions. The SA model is more accurate in attached flows and wakes, including merging boundary layers and wakes. The SA model is somewhat more robust, though for several cases the computational costs are about equal. Considering the uncertainties associated with the experimental data and the use of the RANS approximation, as well as the limitations on the grid resolution that can be used, the performance of these two turbulence models is excellent. They represent the state-of-the-art for this application. The SA model is preferred for general computations of aerodynamic flows, whereas the Menter model is the better choice if separated flows are of primary interest. A summary of the major conclusions of the study could be stated as follows:

- SA and SST models yielded generally similar results.
- Not surprisingly, grid sizes tended to increase in density from less than $50,000$ points to about triple such size as the decade advanced. Many independent grid studies seemed to suggest that 50,000 points may be sufficient to resolve surface pressures, but flow field quantities such as velocity profiles require significantly more grid points. Some estimates indicate that, at least, 100,000 to 200,000 elements are required, unless a scheme with higher order spatial accuracy is employed. Grid issues tend to still remain very important in general. Those references that exercise the greatest care in ensuring high-quality, sufficiently refined grids with an accurate representation of the wind tunnel geometry tended to produce the best correlations with experiment. Underresolution in key areas, such as wakes, can lead to overdissipation and incorrect conclusions. Moreover, for 2-D computations, it is important to have a farfield grid extent of, at least, 50 to 60 chords or, otherwise, special farfield boundary condition treatment is required in order to accurately predict drag (Basso *et al.*, 2006). The inclusion of tunnel walls in the computations appears to be increasingly important at higher angles of attack.
- Grid distribution is also an important factor: sufficient grid resolution is required in key areas of the flowfield, *e.g.*, wakes and vortices.
- The configuration should be modeled as accurately as possible, *e.g.*, with the inclusion of support brackets, aeroelastic deformations, tunnel walls, chines), or otherwise these effects should be known. Geometry fidelity appears to be more crucial as the angle of attack approaches maximum lift.
- The fine grid was probably sufficiently fine for use at the lower angles of attack. However, its adequacy at higher angles of attack was dubious, particularly because of underresolution of the wall vortex.

Aside from the points listed above, some general conclusions from this work were: (a) 2-D CFD should not be expected to agree with the nominally 2-D wind tunnel experiment at high-lift conditions because the experiment looses its 2-D characteristics at high angles of attack, and (b) 3-D CFD using the current grids and methodology compared well with experiment at low angles of attack, but did not adequately model the character of the wind tunnel flow field near maximum lift. To improve this deficiency, based on the present experience, it is recommended that future 3-D CFD efforts include (in order of importance):

- Finer grid resolution in the region of the wall vortex, and overall finer resolution for unstructured grids;
- Top and bottom walls, and mounting brackets;
- Better characterization of the incoming side-wall boundary layer.

6. Acknowledgments

The authors are indebted to Fundação de Amparo à Pesquisa do Estado de São Paulo, FAPESP, which provided support for the work through the Research Grant No. 2000/13768-4. The authors also acknowledge the partial support of Conselho Nacional de Desenvolvimento Científico e Tecnológico, CNPq, through the Integrated Project Research Grants No. 501200/2003-7 and 502053/2004-6.

7. References

Basso, E., Azevedo, J. L. F., Bitencourt, L. O., and Andrade, T. J., São José dos Campos, SP, Brazil, 2006, Cálculo do Escoamento Bidimensional sobre o Perfil RAE 2822 Utilizando o Software CFD++, Relatório do IAE para o Núcleo de CFD, Instituto de Aeronáutica e Espaço.

CFD++, 2005, The CFD++ Computational Fluid Dynamics Software.

den Berg, B. V. and Gooden, J. H. M., 1994, Low-Speed Surface Pressure and Boundary Layer Measurement Data for the NLR 7301 Airfoil Section With Trailing Edge Flap, "A Selection of Experimental Test Cases for the Validation of CFD Codes - AGARD AR-303", Vol. 2, pp. A9–1–A9–12.

Drela, M., 1996, A User's Guide to MSES 2.92.

ICEM, 2005, ANSYS ICEM CFD.

Lima-Silva, A. L. F., Neto, J. A. O., Antunes, A. P., Mendonça, M. T., Azevedo, J. L. F., and Neto, A. S., 2005, Numerical Study of Two-Dimensional High-Lift Configurations Using the MSES Code, "Proceedings of the 18th International Congress of Mechanical Engineering", Ouro Preto, Brazil.

Lovell, D. A., 1977, A Wind-Tunnel Investigation of the Effects of Flap Span and Deflection Angle, Wing Planform and a Body on the High-Lift Performance of a 28° Swept Wing, "Aeronautical Research Council, ARC C.P. 1372", Vol. .

Moir, I. R. M., 1994, Measurements on a Two-Dimensional Aerofoil With High-Lift Devices, "A Selection of Experimental Test Cases for the Validation of CFD Codes - AGARD AR-303", Vol. 2, pp. A9–1–A9–12.

Morrison, J. H., 1998, Numerical Study of Turbulence Model Predictions for the MD 30P/30N and NHLP-2D Three-Element High-lift Configurations, Vol. NASA/CR-1998-208967.

White, F. M., Second edition, 1991, "Viscous Fluid Flow", McGraw-Hill International Editions.

8. Author rights

The authors are the sole responsible for the contents in this paper.